





Activity-induced diffusion recovery in crowded colloidal suspensionsArnab Maiti ¹, Yuki Koyano ², Hiroyuki Kitahata ³, and Krishna Kanti Dey ^{1,*}¹Laboratory of Soft and Living Materials, Department of Physics, Indian Institute of Technology Gandhinagar, Gandhinagar, Gujarat 382055, India²Graduate School of Human Development and Environment, Kobe University, 3-11 Tsurukabuto, Nada-ku, Kobe, Hyogo 657-0011, Japan³Department of Physics, Graduate School of Science, Chiba University, Yayoi-cho 1-33, Inage-ku, Chiba 263-8522, Japan

(Received 7 July 2023; accepted 12 March 2024; published 23 May 2024)

We show that the forces generated by active enzyme molecules are strong enough to influence the dynamics of their surroundings under artificial crowded environments. We measured the behavior of polymer microparticles in a quasi-two-dimensional system under aqueous environment, at various area fraction values of particles. In the presence of enzymatic activity, not only was the diffusion of the suspended particles enhanced at shorter time-scales, but the system also showed a transition from subdiffusive to diffusive dynamics at longer time-scale limits. Similar observations were also recorded with enzyme-functionalized microparticles. Brownian dynamics simulations have been performed to support the experimental observations.

DOI: [10.1103/PhysRevE.109.054607](https://doi.org/10.1103/PhysRevE.109.054607)**I. INTRODUCTION**

Cellular functions usually involve many enzyme-mediated catalytic reactions that control the rate of various chemical transformations [1]. Unlike the biomolecular motors, most enzymes in nature operate in free states and rather diffuse to and away from their substrates during catalytic reactions [2]. For a long time, such molecules were believed neither to have any energy transduction ability during substrate turnover nor to influence significantly the dynamics of their surroundings. In a series of experiments, enzymes have, however, been found to generate forces during substrate turnover in the form of nonthermal active fluctuations, which were significant enough to influence their dynamics and that of their surroundings in aqueous solutions [3–9]. Although the initial diffusion measurements carried out in this regard using fluorescence correlation spectroscopy [3,4,6,10,11] received some criticisms [12–17], experiments conducted with techniques such as total internal reflection fluorescence microscopy [18] validated the significance of the previous observations and highlighted the mechanical energy transduction ability of enzymes. Over the past decade, many theoretical studies have also sought to elucidate the mechanism behind force generation by enzymes in dilute aqueous environments [19–33]. Interestingly, enzymes when immobilized over microscopic particle surface or macroscopic gold patch led to the development of chemically driven micromotor and self-powered micropumps, rendering these systems mechanically active [34–41]. While the observations on enhanced enzyme diffusion were still being deliberated, enzymes were also found to influence the diffusion of nearby passive particles during catalysis [7,9]. The behavior is analogous to the generation of randomly fluctuating forces inside cells by the aggregation and adaptations of molecular motors, which are believed

to drive diffusivelike, nonthermal motion of cellular components, affecting the overall metabolic state of the cell [42–44]. Population of active bacteria has also been observed to considerably affect the dynamics of their surroundings either by direct interactions (hydrodynamic coupling) [45], collisions [46], or by changing the fluid rheology considerably [47–50]. The observations however, provide strong motivation to investigate if enzymes, while catalyzing various chemical reactions within intracellular crowded environments, could generate sufficient mechanical forces to influence the motion of nearby particles. A positive answer to this will refine our understanding of organelle and small molecules' motion in cells and underscore fundamental principles of molecular transport, assembly, and motility under crowded cytoplasmic environments [51,52]. Herein, we demonstrate that forces generated by enzymatic reactions are sufficiently long ranged and strong enough to influence the dynamics of their surroundings, under artificial crowded environments. This was demonstrated by using crowded colloidal suspensions of 3 μm polystyrene particles mixed with solutions of active enzymes such as urease, where the amount of crowding was controlled by changing the area fractions of the suspended microparticles. At shorter time-scale regimes, the passive tracers were found to display diffusive dynamics while at longer time scales, their behavior was found to be subdiffusive. With increased amount of crowding, the diffusion coefficient at shorter time scale and the diffusion exponent at longer time scale decreased gradually, as observed in previous studies [53,54]. However, with the onset of enzymatic reactions in the system (triggered by the addition of calculated amount of substrate solutions from outside), both the diffusion coefficients at shorter time scale and the diffusion exponents at longer time scale were found to increase. The recovery of diffusion values and exponents were likely due to the decrease in effective viscosity and particle caging effect, respectively, both facilitated by the enzyme substrate reactions. Experiments were also conducted with enzyme-coated microparticles, at sufficiently higher area fraction limits. Even on this occasion,

*Author to whom correspondence should be addressed: k.dey@iitgn.ac.in

substrate turnover was found to generate sufficient mechanical force to enhance the diffusivity of the particles and influence their subdiffusive dynamics at longer time scales. We consider both these observations as significant since from a scientific standpoint, although the cooperativity between diffusing enzymes in various intracellular signaling pathways has been well documented, the degree to which their activity plays a role in cellular mechanics has not yet been investigated. Moreover, although it was hypothesized that localized energy transduction by enzymes was capable of generating long-ranged dynamic interactions with their surroundings, even in crowded conditions [31–33], to date, there have been no experimental studies validating such propositions. The previous theoretical work based on Langevin dynamics of active dimers reported implication of particle conformational changes over the transport properties of the system [33], which is similar to the experimental observations recorded with enzyme-coated microparticles in this study. However, to understand the experimental results obtained with passive microparticles in active enzyme suspensions, new simulations have been performed. Our results, therefore, promise a distinct shift in paradigm in molecular biophysics research, whereby localized energy transduction by enzymes is expected to play a crucial role in understanding diffusion-mediated intracellular processes. The catalysis-induced force generation and recovery of particle diffusion under artificial crowded environment may also provide newer insights into the reported stochastic motion of the cytoplasm [42,43], glass transition of cytoplasmic matrix during metabolism [55,56], dynamics of nanoswimmers [57], and convective transport in cells [58,59], opening up new research opportunities in active biomolecular mechanics [60].

II. RESULTS AND DISCUSSIONS

We studied the dynamics of $3\ \mu\text{m}$ polystyrene tracer particles in different volume fractions of colloidal suspension. For the preparation of the experimental solution, $10\ \mu\text{L}$ of the stock solution was serially diluted with DI water (pH 7, resistivity $18.2\ \text{M}\Omega\ \text{cm}$) in the ratio 1:10 in successive stages. All measurements were performed at room temperature ($25\ ^\circ\text{C}$). The prepared colloidal sample was inserted into a custom-built microscopic chamber for the motion study. Commercially procured glass slides were treated with piranha solution followed by a thorough wash and dry. A small circular plastic chamber was then fixed over the glass slide. We employed optical video microscopy and single-particle tracking technique to trace the colloidal particles over the entire field of view in a quasi-two-dimensional (quasi-2D) condition. The schematic of the experimental setup, representative particle suspension images, and trajectory of a tracked particle are shown in Fig. 1. Experimental videos were recorded using a Nikon Eclipse Ti2 Inverted Microscope, with an objective of $60\times$, 10 frames per second. Videos were recorded for a typical period of 10 min for passive cases, and 5 min for active cases. Before recording each video, we waited for a period of 30 min so that the experimental sample mounted on the microscope could reach a steady state and become free from any external perturbations. All frames from each recorded video were then analyzed and tracked through particle tracking codes developed by Crocker and Grier [61]. Mean-squared

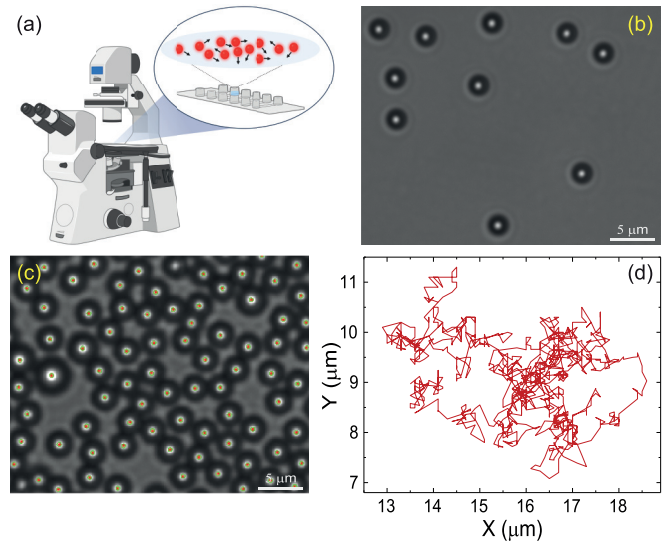


FIG. 1. (a) Schematic of the experimental setup for measuring particle diffusion in quasi-2D geometry (created using BIORENDER). (b) The captured image of colloidal microparticles of area fraction $\phi = 0.03$ (dilute regime). (c) Centroid annotated image of colloidal microparticles of area fraction $\phi = 0.35$ (crowded regime). (d) Trajectory of a colloidal particle generated through particle tracking protocol.

displacement (MSD) and diffusion coefficient were estimated using a self-developed code in MATLAB. The results were plotted and fitted using the software ORIGINPRO to investigate the dynamic behavior of the suspended tracer particles.

To introduce nonthermal active fluctuations in the system, urea urease biochemical reaction was chosen. The reaction is reported to follow Michaelis-Menten kinetics, with the kinetic parameter values estimated at pH 7 and temperature $38\ ^\circ\text{C}$ as follows: $k_{\text{cat}} = 2.34 \times 10^4\ \text{s}^{-1}$ and $K_M = 3.28 \times 10^{-3}\ \text{M}$ [62]. The enthalpy of the reaction has been reported to be $59.6\ \text{kJ mol}^{-1}$ measured in phosphate buffer, at pH 7.5 and temperature $25\ ^\circ\text{C}$ [23,63]. Enzyme assay was carried out using UV-Vis spectroscopy, measuring absorbance of the dye phenol red at $560\ \text{nm}$. Keeping in mind the available experimental time, the concentrations of enzyme and substrate in the final experimental sample were taken to be $10\ \text{nM}$ and $100\ \text{mM}$, respectively, which gave around $300\ \text{s}$ reaction time, at nearly constant reaction rate.

Enzyme functionalization was performed using biotin-streptavidin linkage chemistry [35]. EZ-Link-Maleimide-PEG2-Biotin was used to tag urease where the binding occurred at a pH between 6.5 and 7.5. For confirmation of enzyme functionalization over the polymer surface, we used urease tagged with DyLight 488 Maleimide dye (ex/em: 493/518). Finally, the DyLight tagged urease immobilized microparticles were imaged under fluorescence microscope. The particles were found to be highly fluorescent, suggesting sufficient attachment of enzymes over the bead surfaces.

We measured the MSD of $3\ \mu\text{m}$ polystyrene tracer particles in deionized water for five different area fractions ϕ , typically ranging from 0.02–0.38. Maintaining stable particle area fraction values during the experiments was challenging, as the particles were in motion. To ensure that the experi-

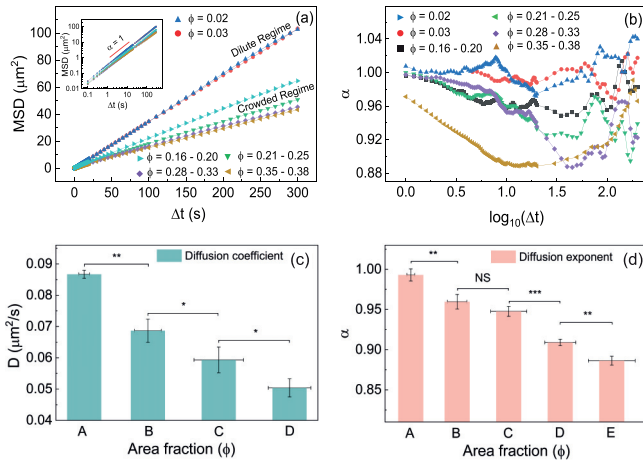


FIG. 2. (a) The MSD profiles of microparticle suspensions without activity for different area fractions. The inset shows the same plots in the log scale. (b) Diffusion exponents α as a function of $\log_{10}(\Delta t)$, which helped in identifying the short and long time-scale regimes. The variation of short time-scale diffusion coefficient and long time-scale diffusion exponent of passive particles for different area fraction values are shown in (c) and (d), respectively. The area fractions corresponding to the different bars are A: 0.03 ± 0.01 , B: 0.13 ± 0.02 , C: 0.21 ± 0.04 , D: 0.28 ± 0.03 , E: 0.38 ± 0.05 . Particles with $\phi = 0.35\text{--}0.38$ did not show any diffusive motion for the entire range of the time steps used, and as such it has not been included in (c). The symbols *, **, *** signify the significance levels of $p < 0.05$, $p < 0.01$, $p < 0.001$, respectively. NS = not significant.

mental measurements were statistically significant, we tracked hundreds of particles in each data set, performed analysis using three independent data sets and conducted necessary control experiments. For low area fractions, particle motion remained mostly diffusive, whereas at higher values of ϕ , the plots showed subdiffusive behavior with gradually decreasing slopes with increasing time steps [Fig. 2(a)]. Considering the MSD changes in the log scale [Fig. 2(a), inset], we observed that for $\phi \leq 0.03$, the motion of the particles remained diffusive at all time steps. For higher values of ϕ , until a time step of 3 s, the particle motion remained diffusive. However, at intermediate time steps (20–50 s) the particle dynamics was dominated by the crowding in the system making their motion subdiffusive in nature. Interestingly, at the highest area fraction ($\phi = 0.35\text{--}0.38$) limit, the particles did not show any diffusive motion for the entire range of the time steps used. At sufficiently longer time steps, the particle motion became diffusive again. To identify short and long time-scale diffusion coefficients and intermediate subdiffusion regimes [64,65], we generated $\log_{10}(\text{MSD}/\Delta t)$ vs $\log_{10}(\Delta t)$ plots that are provided in Appendix A. These observations were further confirmed by calculating $d \log_{10}(\text{MSD})/d \log_{10}(\Delta t)$ (which yielded the corresponding diffusion exponent α) and plotting it as a function of $\log_{10}(\Delta t)$ [Fig. 2(b)]. For data analysis, we considered the time intervals $\Delta t = 1\text{--}3$ s as the short time-scale regime where the motion remained diffusive. The intervals $\Delta t = 20\text{--}50$ s were chosen as the long time-scale regime where the crowding effect dominated. The diffusion coefficients and subdiffusion exponents were calculated from three independent sets of MSD measurements, under identi-

cal experimental conditions. In dilute particle concentration limit, the diffusion coefficient of $3 \mu\text{m}$ polystyrene particles was measured to be $0.088 \mu\text{m}^2/\text{s}$. However, from the Stokes-Einstein relation the diffusion coefficient was estimated to be $0.14 \mu\text{m}^2/\text{s}$ for the same particle at room temperature $T = 25^\circ\text{C}$ in water (viscosity $\eta = 0.001 \text{ Pa s}$). Therefore, the experimentally measured diffusion coefficient was nearly 37% less than the expected value for infinite dilution. This could be explained by considering the effect of the bottom surface and corresponding hindrance in particle diffusion [66,67]. The negatively charged microparticles could interact with the negatively charged surface [68,69], and in the presence of gravity, it might lead to the restricted diffusion of the former (see Appendix B). We also estimated the increase in effective viscosity of the particle suspension given by $\eta(\phi) = \eta_0(1 + 2.5\phi)$ [70] and hypothesized that the observed decrease in the diffusion coefficient at the shorter time-scale regime was due to the increase in effective viscosity with higher area fraction ϕ [Fig. 2(c)]. The supporting calculations are given in Appendix C, considering D_{dilute} and η_{dilute} as the diffusion coefficient of tracers and solution viscosity at dilute concentration limit ($\phi = 0.03$). We also hypothesized that the increased ϕ resulted in greater degree of caging effect [71,72] at longer time-scale regimes, resulting in lowering the subdiffusive exponent α with ϕ , as observed [Fig. 2(d)]. From the above results, it became clear that crowding in a colloidal system could significantly influence both the short time-scale diffusion coefficients and long time-scale diffusion exponents of the suspended particles. Importantly, diffusion of species in two-dimensional systems under crowded environments are of immense importance due to their potential implications in cellular transport under confinement and in the dynamics of membrane proteins. Although the notion of anomalous diffusion in cells resulting from macromolecular crowding has been opposed by some researchers [73], several experimental [53,74–76] and theoretical studies [77–80] have been conducted in this direction confirming the effect of crowding in facilitating anomalous diffusion in two dimensions. The onset of anomalous diffusion and the mechanism behind the behavior crossover have, however, been not understood very clearly. Specific experimental investigations such as those conducted by Horton *et al.* demonstrated onset of anomalous diffusion of membrane proteins beyond a protein coverage of 5% [76]. Saxton introduced a minimalist model for transport in cellular membranes, wherein for mobile obstacles over a two-dimensional lattice, diffusion was shown to be anomalous over short distances and normal over long distances. The anomalous diffusion exponent and the crossover length were found to increase with the obstacle concentration [78]. To check if enzymatic catalysis could generate sufficient forces to counter this subdiffusive behavior and restore the diffusive dynamics of the system under crowded conditions, we performed experiments both with tracers suspended in active enzyme solutions and high concentrations of enzyme functionalized microparticles in substrate-rich media. A recent study has demonstrated enhanced propulsion of catalase powered motor confined within giant unilamellar vesicles [34], wherein we showed in this study that similar enhancement in motion could also be realized for passive particles suspended in active crowded environment. We selected molecules of

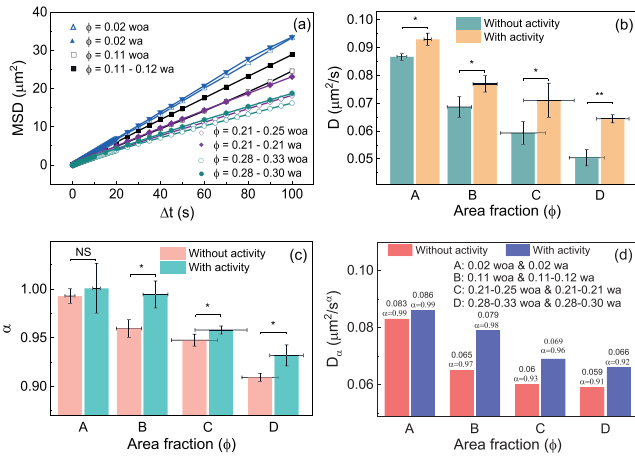


FIG. 3. (a) The MSD profiles of microparticle suspensions for different area fractions in the presence (wa) and absence (woa) of free enzyme activity in the system. The variation of short time-scale diffusion coefficient and long time-scale diffusion exponent of passive particles in active urease solution, for different area fraction values of the particles are shown in (b) and (c), respectively. The area fractions corresponding to the different bars are A: 0.03 ± 0.01 , B: 0.13 ± 0.02 , C: 0.21 ± 0.04 , D: 0.28 ± 0.03 (without activity) and A: 0.02 ± 0.01 , B: 0.12 ± 0.02 , C: 0.17 ± 0.03 , D: 0.26 ± 0.03 (with activity). (d) Subdiffusion coefficients D_α at various area fraction values [corresponding to the MSD plots shown in (a)]. The symbols *, ** signify the significance levels of $p < 0.05$, $p < 0.01$, respectively. NS = not significant.

active urease as nanomotors in our system owing to their robustness, and high substrate turnover rate at room temperature. As both ensemble and time averages were considered for MSD calculations, care was taken to fix the reaction rate that allowed the catalytic reaction to continue for a significant duration. Also, the enzyme substrate concentrations were chosen in such a manner that ensured sufficient substrate turnover and generation of nearly constant mechanical forces during the entire measurement period. Under crowding conditions, the MSD showed enhanced tracer dynamics in the presence of enzymatic activity [Fig. 3(a)]. To observe the change in the diffusive parameters in presence of substrate turnover, we measured the particle diffusion coefficients at shorter time scales (1–3 s), and diffusion exponents at longer time scales (20–50 s) and compared them with those measured in absence of catalysis. Figure 3(b) shows the diffusion coefficients measured at different crowding conditions in the presence and absence of enzymatic activity. The active fluctuations generated by free enzymes in solution was found to enhance the tracer diffusion by nearly 7–27%. Although the exact mechanism of tracer diffusion enhancement is yet to be understood, it is expected to be due to the mechanical energy transferred from the active enzymes to the tracers, facilitated by the media. At longer time-scale regimes, the diffusion exponents of the particles showed a nearly 1–4% enhancement, in the presence of catalytic activity [Fig. 3(c)]. The corresponding subdiffusion coefficients [81] are given in Fig. 3(d). Diffusion of particles measured in only enzyme and only substrate solutions did not show such changes. This indicated that in the presence of force generated due to substrate catalysis, the

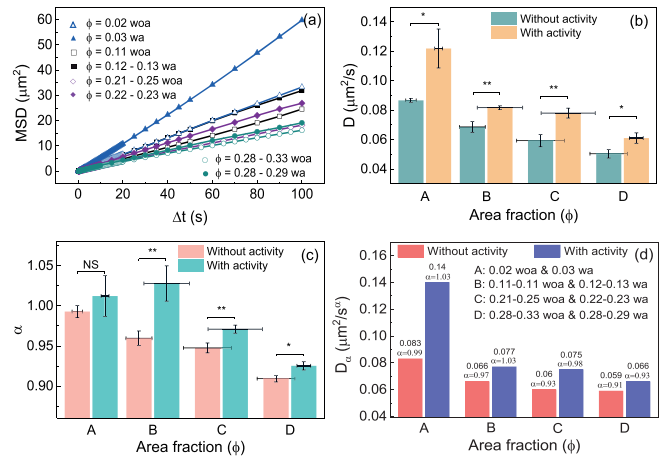


FIG. 4. (a) The MSD profiles of enzyme-immobilized microparticle suspensions for different area fractions in the presence (wa) and absence (woa) of substrate solution in the system. The variation of short time-scale diffusion coefficient and long time-scale diffusion exponent of passive particles functionalized with active urease, for different area fraction values of the particles are shown in (b) and (c), respectively. The area fractions corresponding to the different bars are A: 0.03 ± 0.01 , B: 0.13 ± 0.02 , C: 0.21 ± 0.04 , D: 0.28 ± 0.03 (without activity) and A: 0.03 ± 0.01 , B: 0.11 ± 0.03 , C: 0.18 ± 0.04 , D: 0.28 ± 0.01 (with activity). (d) Subdiffusion coefficients D_α at various area fraction values [corresponding to the MSD plots shown in (a)]. The symbols *, ** signify the significance levels of $p < 0.05$, $p < 0.01$, respectively. NS = not significant.

particles were able to get themselves freed from the crowding effects imposed by their neighbors and displayed enhanced diffusive dynamics. To confirm that the free enzymes did not adsorb over the polymer bead surface during experiments and influenced their propulsion, we also performed experiments with microparticles coated with a thin layer of bovine serum albumin (BSA), which also showed similar enhancement in particle motion during catalysis. It was also noted that upon complete depletion of the substrate in the experimental chamber, both the tracer diffusion at short time-scale regime and diffusion exponent in the long time-scale regime decreased again, like in passive crowded suspensions, indicating that the particles started feeling the effect of crowding in absence of the force generated by the enzymes. Like molecules of free enzymes, microparticles coated with immobilized active enzymes have also been reported to behave as motors and display nontrivial collective dynamics [35]. Instead of using free enzyme molecules as mechanical energy sources to counter the effect of crowding, we used an assembly of urease functionalized active microparticles and investigated if during substrate turnover, the particles could generate forces to overcome their mutual crowding effects. Although theoretical analysis performed earlier suggested such a possibility [33], to the best of our knowledge, it has not yet been demonstrated experimentally. Like passive microparticles suspended in active enzyme solution, the recovery of diffusive dynamics was also observed with active microparticles in different crowding conditions. The microparticles were functionalized with active urease enzymes using biotin streptavidin linkage chemistry. Diffusion studies were performed using different

area fractions of particles that corresponded to different degrees of crowding. Figure 4(a) shows the MSD plots of the particles while Figs. 4(b) and 4(c) show the short time-scale diffusion coefficients and long time-scale diffusion exponents measured at different area fractions. Clearly, like the particle in active enzyme suspensions, the enzyme functionalized particles were able to generate sufficient mechanical forces, overcome the effect of crowding to a significant degree, and restore their diffusive dynamics. In case of enzyme-coated particles, the short time-scale diffusion coefficients was found to get enhanced by approximately 20–40% in the presence of substrate catalysis, while the long time-scale diffusion exponents increased by nearly 2–7%. The corresponding subdiffusion coefficients are given in Fig. 4(d). From the experimental results, we therefore concluded that substrate catalysis by active enzyme molecules generated sufficiently large forces that could influence the dynamics of their surroundings under artificial crowded conditions. The effective viscosity estimated at the short time-scale regime due to crowding was found to be in the range of cytoplasmic viscosity [51,82]. The enhanced diffusion of particles observed at this time-scale regime indicated that the force generated due to catalytic turnover was able to lower the effective viscosity, thereby enhancing the particle propulsion.

III. NUMERICAL STUDIES

To understand the diffusion enhancement of passive tracers by the active enzymes as shown in Fig. 3 from the microscopic viewpoint, we considered a two-dimensional model composed of disk-shaped tracers surrounded by dumbbell-shaped particles [Fig. 5(a)]. The catalytic enzymes changed their shape due to the binding of substrate and returned to the original configuration after the reaction. As the simplest approximation for the changes in the enzymes' conformation, we modeled them as dumbbells cyclically changing their shape. Hereafter, the dumbbell-shaped particles are called the dimers. The mathematical formulation corresponding to the tracer dynamics in active dimer suspension is as follows. In

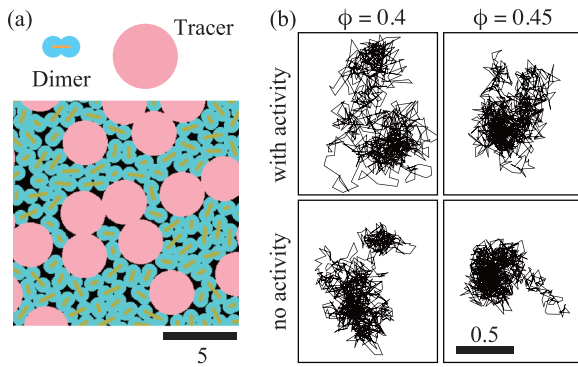


FIG. 5. (a) Snapshot of the suspension composed of the tracer (pink particles) and the dimers (light blue particles connected by yellow bonds). (b) Trajectories of the tracer particles. A spread out (compact) trajectory are observed in the case for the lower (higher) area fraction with (without) activity, which reflects the magnitude of caging effect. The spatial scales for four panels are common.

our model, the Langevin dynamics of the center positions of the tracer particles \mathbf{R}_i and the beads consisting of the dimer $\mathbf{r}_j^{(n)}$ with excluded volume effect were considered, where $i(= 1, \dots, M)$, $j(= 1, \dots, N)$, and $n(= 1, 2)$ indicated the indices for a tracer, dimer, and bead consisting the dimer, respectively. The dynamics of the tracer particles were governed by the following overdamped Langevin equation:

$$\frac{d\mathbf{R}_i}{dt} = -\mu_t \frac{\partial U}{\partial \mathbf{R}_i} + \xi_{t,i}(t) \quad (1)$$

where μ_t was the mobility. The term $\xi_{t,i}$ was the thermal noise, which satisfied $\langle \xi_{t,i,\alpha}(t) \rangle = 0$ and $\langle \xi_{t,i,\alpha}(t) \xi_{t,j,\beta}(s) \rangle = 2\mu_t k_B T \delta_{ij} \delta_{\alpha\beta} \delta(t-s)$ ($\alpha, \beta = x, y$). The function U denoted the potential reflecting the excluded volume effect of particles

$$U = \frac{1}{2} \sum_{i=1}^N \sum_{j(\neq i)=1}^N \sum_{m=1}^2 \sum_{n=1}^2 u(|\mathbf{r}_i^{(m)} - \mathbf{r}_j^{(n)}|; 2r_0) + \frac{1}{2} \sum_{i=1}^M \sum_{j(\neq i)=1}^M u(|\mathbf{R}_i - \mathbf{R}_j|; 2R_0) + \sum_{i=1}^N \sum_{j=1}^M \sum_{m=1}^2 u(|\mathbf{r}_i^{(m)} - \mathbf{R}_j|; r_0 + R_0) \quad (2)$$

where

$$u(r; \rho_0) = \begin{cases} u_0(\rho_0 - r)^2, & (r < \rho_0) \\ 0, & (r > \rho_0) \end{cases} \quad (3)$$

Here, R_0 and r_0 were the radii of the tracer and the bead consisting the dimers, respectively. Thus, the first term in the right-hand side of Eq. (1) represented the repulsive force during particle collision. In the same way, the dynamics of the dimer were given by the following over-damped Langevin equation:

$$\frac{d\mathbf{r}_i^{(n)}}{dt} = -\mu \frac{\partial E_i}{\partial \mathbf{r}_i^{(n)}} - \mu \frac{\partial U}{\partial \mathbf{r}_i^{(n)}} + \xi_i^{(n)}(t) \quad (4)$$

where μ was the mobility. The term $\xi_i^{(n)}$ was the thermal noise, which satisfied $\langle \xi_{i,\alpha}^{(m)}(t) \rangle = 0$, $\langle \xi_{i,\alpha}^{(m)}(t) \xi_{j,\beta}^{(n)}(s) \rangle = 2\mu k_B T \delta_{mm} \delta_{ij} \delta_{\alpha\beta} \delta(t-s)$. It should be noted that the particle mobilities hold the relation $\mu = R_0 \mu_t / r_0$ from the Stokes' law. The first term in the right-hand side of Eq. (4) expressed the force between the beads composing a dimer, where

$$E_i(t) = \frac{k}{2} (|\mathbf{r}_i^{(1)} - \mathbf{r}_i^{(2)}| - \ell_i(t))^2 \quad (5)$$

In the numerical calculations, we compared two cases: one is that the length of the dimer, $\ell_i(t)$, changed in time, which corresponded to the conformation changes in the enzymes. Specifically, it changed as follows:

$$\ell_i(t) = \ell_0 + \ell_1 \sin \psi_i(t) \quad (6)$$

$$\frac{d\psi_i}{dt} = \omega + \zeta_i(t) \quad (7)$$

where $\zeta_i(t)$ was the white Gaussian noise with $\langle \zeta_i(t) \zeta_j(s) \rangle = 2\eta \delta_{ij} \delta(t-s)$. The phase ψ_i had no correlation among

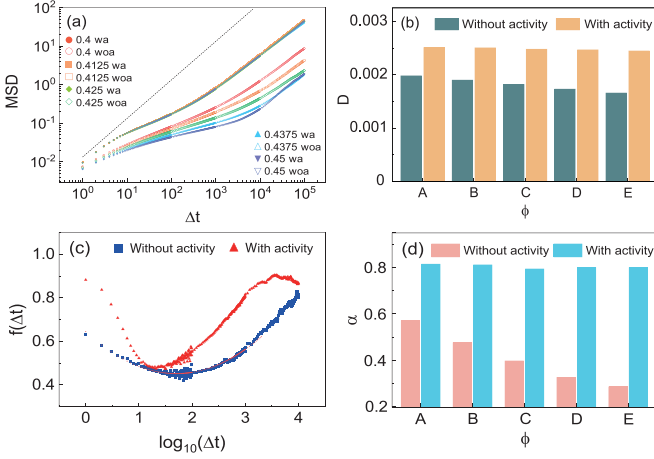


FIG. 6. (a) Variation of MSD against time interval Δt . The MSD plots recorded in the presence of dimer activity are almost superimposed over one another. The straight line (dotted line) indicates the theoretical estimation for the case without any collision. (b) Dependence of diffusion coefficient D on the area fraction and activity. (c) The derivative of $\log_{10}(\text{MSD})$ plotted against $\log_{10}(\Delta t)$. The cases with the area fraction $\phi = 0.4$ are exemplified. (d) Subdiffusion exponent α depending on the area fraction ϕ . In (b) and (d) the area fractions are A: 0.4, B: 0.4125, C: 0.425, D: 0.4375, E: 0.45.

the dimers, which represented that the catalytic reactions occurred incoherently.

In our model, a single dumbbell dissipated energy

$$E = \frac{\pi \omega k^2 \mu \ell_1^2}{k^2 \mu^2 + \omega^2} \quad (8)$$

during a period of the shape change [33]. As seen in Eq. (8), the energy dissipation is a monotonically increasing function of the amplitude ℓ_1 of the conformational change, and thus we considered ℓ_1 as the parameter that tuned the activity of the system.

The spatial scale was normalized by the bead radius comprising a dimer, r_0 . The radius of the tracer particle was $R_0 = 3$, and the dimer's natural length was $\ell_0 = 1.5$. The time was scaled by the damping of the bead consisting of a dimer, i.e., $\mu = 1$. Other parameters were set to be $u_0 = 1$, $k = 1$, $\omega = 0.1$, $k_B T = 0.01$, and $\eta = 0.1$. The amplitude of the oscillation was set to be $\ell_1 = 1$ and 0, which corresponded to the active and nonactive cases, respectively. The area fraction of dimer was fixed to be 0.5, and that of tracer particles was changed as 0.4, 0.4125, 0.425, 0.4375, and 0.45. By increasing the area fraction, the trajectory of the tracer particle became increasingly compact, while the activity made the trajectory broader, as shown in Fig. 5(b). To elucidate this further, the MSDs of the tracer particles as a function of time intervals were obtained by averaging over all tracer particles. As seen in Fig. 6(a), the MSDs became smaller for larger area fractions of tracer particles in the absence of any dimer activity. The diffusion coefficient determined by the MSD at $\Delta t = 1$ is shown in Fig. 6(b). Since the diffusion coefficient should coincide with $D_{\text{theory}} = \mu_r k_B T = 10^{-2}/3$ for the limit of $\Delta t \rightarrow 0$, the crowding effect already appeared at $\Delta t = 1$. To check the subdiffusion regime, the local gradient of MSD,

$f(\Delta t) = d[\log_{10}(\text{MSD}(\Delta t))]/d(\log_{10} \Delta t)$ was checked. The examples of $f(\Delta t)$ are plotted in Fig. 6(c), which are qualitatively similar to the experimental results in Fig. 2(b). The subdiffusion exponent was determined by the gradient of MSD at $\Delta t = 10^3$, since the characteristic time scale at which the subdiffusion regime appeared was around $\Delta t = 10^3$ [Fig. 6(a)]. As shown in Fig. 6(d), the subdiffusion exponent α estimated in the presence of activity always exceeded that estimated without dimer activity. Moreover, the subdiffusion exponent was a decreasing function of the area fraction of tracer particles for nonactive cases. Such a trend was qualitatively similar to the experimental results. The experimental and simulated subdiffusion regimes were identified from the $\log_{10}(\text{MSD}/\Delta t)$ vs $\log_{10}(\Delta t)$ plots that are shown in Fig. 7, Appendix A. Simulations were performed over an extended range of particle area fractions, including those used in experiments, which yielded similar behavior (Fig. 8, Appendix D). From the numerical results, we asserted that the conformation changes in the enzymes was essential in deciding the dynamics of tracer particles in active crowded suspensions. The experimentally measured and numerically estimated relative diffusion parameters are given in Figs. 9–11, Appendix E.

IV. CONCLUSIONS

In summary, we demonstrate that the force generated by enzymes during substrate turnover is sufficiently strong to influence the dynamics of their surroundings, under artificially crowded environments. These observations have several important implications and offer opportunities to investigate the consequences of biomolecular activities over transport, assembly, and organization of components under crowded intracellular environments.

ACKNOWLEDGMENTS

K.K.D. thanks SERB, India (ECR/2017/002649, CRG/2023/007588), DST, India (DST/ICD/BRICS/PilotCall3/BioTheraBubble/2019), Ministry of Education, Government of India (MoE-STARS/STARS-2/2023-0620), and IIT Gandhinagar for financial supports. H.K. and Y.K. acknowledge support received from JSPS KAKENHI Grants No. JP21H01004 and No. JP20K14370, respectively. We are thankful to Prof. Alexander S. Mikhailov and Prof. Raymond Kapral for insightful discussions. Help received from Dr. Chandan Kumar Mishra in developing the particle tracking methodology is gratefully acknowledged.

APPENDIX A: OBSERVATION OF SUBDIFFUSIVE DYNAMICS OF PARTICLES AT DIFFERENT AREA FRACTION VALUES

To observe the subdiffusive dynamics of particles under crowded conditions, we plot the variation of $\log_{10}(\text{MSD}/\Delta t)$ against $\log_{10}(\Delta t)$, for different area fractions as shown in Fig. 7. The subdiffusive regimes in these plots are characterized by a decreasing slope with increasing time steps, gradually leveling off to zero [64,65].

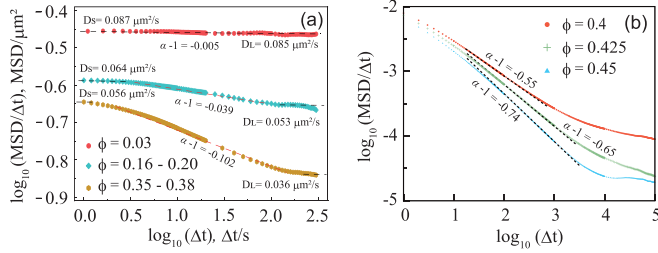


FIG. 7. (a) Variation of $\log_{10}(\text{MSD}/\Delta t)$ against $\log_{10}(\Delta t)$ with different area fractions of the passive tracers in the experimental system. (b) Numerically estimated plots of $\log_{10}(\text{MSD}/\Delta t)$ against $\log_{10}(\Delta t)$. The area fraction ϕ of the tracers are shown in the figure legend. The dimers in the simulations are considered to be inactive.

APPENDIX B: HINDERED DIFFUSION OF PARTICLES NEAR THE BOTTOM SURFACE OF THE EXPERIMENTAL SAMPLE CHAMBER

The experimentally measured diffusion coefficient of 3 μm polystyrene particle was nearly 37% less than that predicted by the Stokes-Einstein relation. This could be explained by considering the effect of the bottom surface and corresponding hindrance in particle diffusion [66,67]. The negatively charged microparticles interacted with the bottom surface, which also had a negative surface charge (due to the dissociation of terminal silanol groups) [68,69]. Therefore, near the bottom surface of the experimental chamber, the microparticles were influenced by the combined effects of gravitational, van der Waals, and Coulomb interactions, which helped in stabilizing them at a certain height, with a diffusion coefficient determined by the separation of the microparticles from the bottom of the chamber h and their radius r . Fauchaux *et al.* [67] estimated this hindered diffusion using the dimensionless length scale parameter $\gamma = (h - r)/r$. With $h \sim 5 \mu\text{m}$ and $r = 1.5 \mu\text{m}$, this gave the estimated hindered diffusion value in our case to be $0.093 \mu\text{m}^2/\text{s}$, which matched well with our experimental results.

APPENDIX C: EFFECTIVE VISCOSITY AND RELATIVE DIFFUSION OF PARTICLES AT DIFFERENT AREA FRACTION VALUES

The table below illustrates that as the area fraction (ϕ) of particles increases, the effective viscosity of the system also

Area fraction (ϕ)	Diffusion coefficient (D) ($\mu\text{m}^2\text{s}^{-1}$)	Relative diffusion coefficient (D_{dilute}/D)	$D_{\text{dilute}}/D = \eta/\eta_{\text{dilute}} = 1 + 2.5\phi$
0.03	0.088	1	1.08
0.16–0.20	0.065	1.35	1.45
0.21–0.25	0.054	1.63	1.58
0.28–0.33	0.050	1.76	1.75

increases. Here, D_{dilute} and η_{dilute} represent the diffusion coefficient of tracers and the solution viscosity at dilute particle concentration limit ($\phi = 0.03$).

APPENDIX D: SIMULATED DEPENDENCE OF DIFFUSION DYNAMICS OF THE PARTICLES ON THEIR AREA FRACTIONS AND THE ACTIVITY OF THE SYSTEM

In experiments, the number of the enzymes was relatively much higher than the number of tracer particles. It was therefore challenging to simulate the systems including dimers (enzymes) and tracer particles with similar number ratios. However, if the enzymes, by actively changing their shape exert an exclusive force on a tracer particle by multiple collisions, within a certain short time range, this could be replaced with a single collision, though it is difficult to estimate the magnitude of the force involved in such a process. Therefore, for the numerical simulations, we focused on capturing the qualitative essence of the anomalous diffusion observed in the experiments and considered a size ratio of the dimer to the tracer particle, different than that in the actual system. The parameters were set so that the effect of activity in enzymes can be observed clearly. The number density of particles was also assumed higher in simulations compared to that in experiments. We, however, confirmed that for the entire particle density range used, we obtain qualitatively the same behavior for diffusion coefficients and exponents similar to that observed in the experiments. The diffusion coefficients and the subdiffusion exponents were decreasing function of the area fraction, the values of which in the presence of dimer activity always exceeded that for the nonactive cases as shown in Fig. 8.

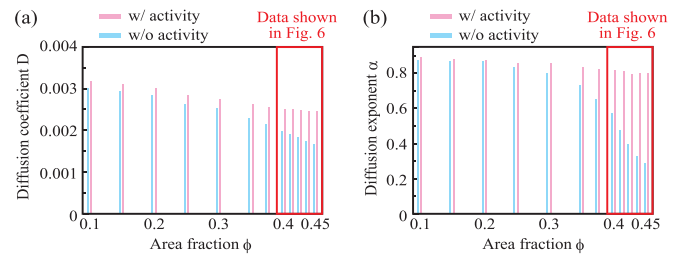


FIG. 8. Numerical results for the wide range of the area fraction of the tracers. (a) The short time-scale diffusion coefficient and (b) long time-scale diffusion exponent values are shown. In the results and discussion section above, the data shown in the red boxes are included. Importantly, diffusion coefficient and exponent values estimated at lower area fractions of tracers show similar variations as that observed in experiments.

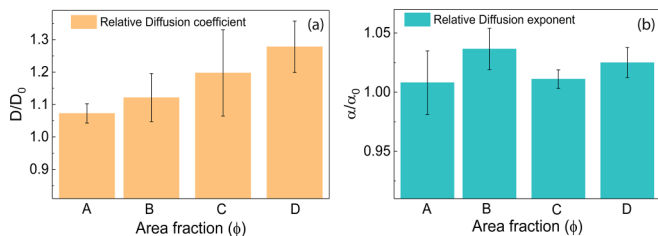


FIG. 9. (a) Relative diffusion coefficients at short time-scale regimes and (b) relative diffusion exponents at long time-scale regimes of passive tracers in active urease suspension at different area fraction values. The measured area fractions for passive cases are A: 0.03 ± 0.01 , B: 0.13 ± 0.02 , C: 0.21 ± 0.04 , D: 0.28 ± 0.03 , and those for the active cases are A: 0.02 ± 0.01 , B: 0.12 ± 0.02 , C: 0.17 ± 0.03 , D: 0.26 ± 0.03 .

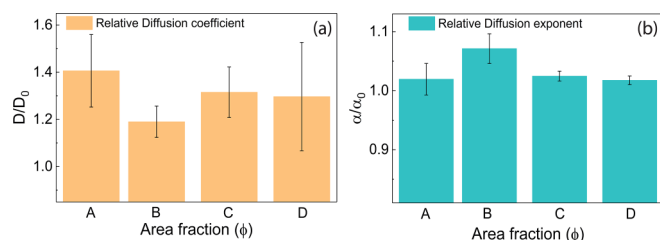


FIG. 10. (a) Relative diffusion coefficients at short time-scale regimes and (b) relative diffusion exponents at long time-scale regimes of enzyme functionalized micro particles at different area fraction values. The measured area fractions for passive cases are A: 0.03 ± 0.01 , B: 0.13 ± 0.02 , C: 0.21 ± 0.04 , D: 0.28 ± 0.03 , and those for the active cases are A: 0.03 ± 0.01 , B: 0.11 ± 0.03 , C: 0.18 ± 0.04 , D: 0.28 ± 0.01 .

APPENDIX E: EXPERIMENTALLY MEASURED AND NUMERICALLY ESTIMATED RELATIVE DIFFUSION COEFFICIENTS AND SUBDIFFUSION EXPONENTS OF PARTICLES

Case 1: For passive microparticles in active urease suspension (Fig. 9).

Case 2: For urease coated microparticle suspension in substrate-rich media (Fig. 10).

Case 3: For disk-shaped tracers in a population of active dimers (Fig. 11).

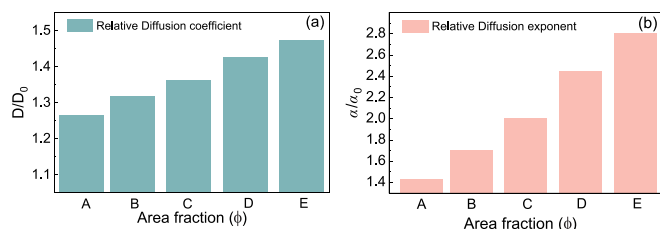


FIG. 11. (a) Relative diffusion coefficients at the short time-scale regimes and (b) relative diffusion exponents at long time-scale regimes calculated through numerical simulations. The area fractions corresponding to the different bars are A: 0.4, B: 0.4125, C: 0.425, D: 0.4375, E: 0.45.

- [1] G. M. Cooper and R. E. Hausman, *The Cell: A Molecular Approach*, 4th ed. (ASM Press, Washington DC, 2007).
- [2] P. J. Butler, K. K. Dey, and A. Sen, *Cell. Mol. Bioeng.* **8**, 106 (2015).
- [3] H. S. Muddana, S. Sengupta, T. E. Mallouk, A. Sen, and P. J. Butler, *J. Am. Chem. Soc.* **132**, 2110 (2010).
- [4] S. Sengupta, K. K. Dey, H. S. Muddana, T. Tabouillot, M. E. Ibele, P. J. Butler, and A. Sen, *J. Am. Chem. Soc.* **135**, 1406 (2013).
- [5] S. Sengupta, M. M. Spiering, K. K. Dey, W. Duan, D. Patra, P. J. Butler, R. D. Astumian, S. J. Benkovic, and A. Sen, *ACS Nano* **8**, 2410 (2014).
- [6] P. Illien, X. Zhao, K. K. Dey, P. J. Butler, A. Sen, and R. Golestanian, *Nano Lett.* **17**, 4415 (2017).
- [7] X. Zhao, K. K. Dey, S. Jeganathan, P. J. Butler, U. M. Córdova-Figueroa, and A. Sen, *Nano Lett.* **17**, 4807 (2017).
- [8] A.-Y. Jee, Y.-K. Cho, S. Granick, and T. Tlusty, *Proc. Natl. Acad. Sci. USA* **115**, E10812 (2018).
- [9] X. Lin and Y. He, *Anal. Chem.* **94**, 7158 (2022).
- [10] A.-Y. Jee, T. Tlusty, and S. Granick, *Proc. Natl. Acad. Sci. USA* **117**, 29435 (2020).
- [11] A.-Y. Jee, S. Dutta, Y.-K. Cho, T. Tlusty, and S. Granick, *Proc. Natl. Acad. Sci. USA* **115**, 14 (2018).
- [12] A.-Y. Jee, K. Chen, T. Tlusty, J. Zhao, and S. Granick, *J. Am. Chem. Soc.* **141**, 20062 (2019).
- [13] Z. Chen, A. Shaw, H. Wilson, M. Woring, X. Darzacq, S. Marqusee, Q. Wang, and C. Bustamante, *Proc. Natl. Acad. Sci. USA* **117**, 21328 (2020).
- [14] Y. Zhang, M. J. Armstrong, N. M. B. Kazeruni, and H. Hess, *Nano Lett.* **18**, 8025 (2018).
- [15] J.-P. Günther, M. Börsch, and P. Fischer, *Acc. Chem. Res.* **51**, 1911 (2018).
- [16] X. Bai and P. G. Wolynes, *J. Chem. Phys.* **143**, 165101 (2015).
- [17] J.-P. Günther, G. Majer, and P. Fischer, *J. Chem. Phys.* **150**, 124201 (2019).
- [18] M. Xu, J. L. Ross, L. Valdez, and A. Sen, *Phys. Rev. Lett.* **123**, 128101 (2019).
- [19] T. Sakaue, R. Kapral, and A. S. Mikhailov, *Eur. Phys. J. B* **75**, 381 (2010).
- [20] A. Cressman, Y. Togashi, A. S. Mikhailov, and R. Kapral, *Phys. Rev. E* **77**, 050901(R) (2008).
- [21] R. Golestanian, *Phys. Rev. Lett.* **105**, 018103 (2010).
- [22] S. Pressé, *Proc. Natl. Acad. Sci. USA* **117**, 32189 (2020).
- [23] C. Riedel, R. Gabizon, C. A. M. Wilson, K. Hamadani, K. Tsekouras, S. Marqusee, S. Pressé, and C. Bustamante, *Nature (London)* **517**, 227 (2015).
- [24] R. Golestanian, *Phys. Rev. Lett.* **115**, 108102 (2015).

- [25] P. Illien, T. Adeleke-Larodo, and R. Golestanian, *Europhys. Lett.* **119**, 40002 (2017).
- [26] M. Dennison, R. Kapral, and H. Stark, *Soft Matter* **13**, 3741 (2017).
- [27] R. D. Astumian, *ACS Nano* **8**, 11917 (2014).
- [28] S. Kondrat and M. N. Popescu, *Phys. Chem. Chem. Phys.* **21**, 18811 (2019).
- [29] Y. Hosaka, S. Komura, and A. S. Mikhailov, *Soft Matter* **16**, 10734 (2020).
- [30] M. Feng and M. K. Gilson, *Biophys. J.* **116**, 1898 (2019).
- [31] A. S. Mikhailov and R. Kapral, *Proc. Natl. Acad. Sci. USA* **112**, E3639 (2015).
- [32] R. Kapral and A. S. Mikhailov, *Physica D* **318–319**, 100 (2016).
- [33] Y. Koyano, H. Kitahata, and A. S. Mikhailov, *Europhys. Lett.* **128**, 40003 (2019).
- [34] S. Song, A. Llopis-Lorente, A. F. Mason, L. K. E. A. Abdelmohsen, and J. C. M. van Hest, *J. Am. Chem. Soc.* **144**, 13831 (2022).
- [35] K. K. Dey, X. Zhao, B. M. Tansi, W. J. Méndez-Ortiz, U. M. Córdova-Figueroa, R. Golestanian, and A. Sen, *Nano Lett.* **15**, 8311 (2015).
- [36] X. Ma, A. Jannasch, U.-R. Albrecht, K. Hahn, A. Miguel-López, E. Schäffer, and S. Sánchez, *Nano Lett.* **15**, 7043 (2015).
- [37] S. Ghosh, F. Mohajerani, S. Son, D. Velegol, P. J. Butler, and A. Sen, *Nano Lett.* **19**, 6019 (2019).
- [38] T. Patino, A. Porchetta, A. Jannasch, A. Lladó, T. Stumpp, E. Schäffer, F. Ricci, and S. Sánchez, *Nano Lett.* **19**, 3440 (2019).
- [39] S. Sengupta, D. Patra, I. Ortiz-Rivera, A. Agrawal, S. Shklyae, K. K. Dey, U. Córdova-Figueroa, T. E. Mallouk, and A. Sen, *Nature Chem.* **6**, 415 (2014).
- [40] I. Ortiz-Rivera, T. M. Courtney, and A. Sen, *Adv. Funct. Mater.* **26**, 2135 (2016).
- [41] I. Ortiz-Rivera, H. Shum, A. Agrawal, A. Sen, and A. C. Balazs, *Proc. Natl. Acad. Sci. USA* **113**, 2585 (2016).
- [42] M. Guo, A. J. Ehrlicher, M. H. Jensen, M. Renz, J. R. Moore, R. D. Goldman, J. Lippincott-Schwartz, F. C. Mackintosh, and D. A. Weitz, *Cell* **158**, 822 (2014).
- [43] C. P. Brangwynne, G. H. Koenderink, F. C. MacKintosh, and D. A. Weitz, *J. Cell Biol.* **183**, 583 (2008).
- [44] A. K. Rai, A. Rai, A. J. Ramaiya, R. Jha, and R. Mallik, *Cell* **152**, 172 (2013).
- [45] X.-L. Wu and A. Libchaber, *Phys. Rev. Lett.* **84**, 3017 (2000).
- [46] E. W. Burkholder and J. F. Brady, *Phys. Rev. E* **95**, 052605 (2017).
- [47] Y. Hatwalne, S. Ramaswamy, M. Rao, and R. A. Simha, *Phys. Rev. Lett.* **92**, 118101 (2004).
- [48] S. Rafai, L. Jibuti, and P. Peyla, *Phys. Rev. Lett.* **104**, 098102 (2010).
- [49] A. Sokolov and I. S. Aranson, *Phys. Rev. Lett.* **103**, 148101 (2009).
- [50] A. G. McDonnell, T. C. Gopesh, J. Lo, M. O'Bryan, L. Y. Yeo, J. R. Friend, and R. Prabhakar, *Soft Matter* **11**, 4658 (2015).
- [51] K. Luby-Phelps, *Int. Rev. Cytol.* **192**, 189 (1999).
- [52] K. Jacobson and J. Wojcieszyn, *Proc. Natl. Acad. Sci. USA* **81**, 6747 (1984).
- [53] D. S. Banks and C. Fradin, *Biophys. J.* **89**, 2960 (2005).
- [54] M. Weiss, M. Elsner, F. Kartberg, and T. Nilsson, *Biophys. J.* **87**, 3518 (2004).
- [55] B. R. Parry, I. V. Surovtsev, M. T. Cabeen, C. S. O'Hern, E. R. Dufresne, and C. Jacobs-Wagner, *Cell* **156**, 183 (2014).
- [56] N. Oyama, T. Kawasaki, H. Mizuno, and A. Ikeda, *Phys. Rev. Res.* **1**, 032038(R) (2019).
- [57] A. K. Tripathi and T. Tlusty, *Phys. Rev. Lett.* **129**, 254502 (2022).
- [58] E. L. Elson, *Traffic* **2**, 789 (2001).
- [59] J. Rouwkema, B. F. J. M. Koopman, C. A. V. Blitterswijk, W. J. A. Dhert, and J. Malda, *Biotech. Genet. Eng. Rev.* **26**, 163 (2009).
- [60] G. Bao, *J. Mech. Phys. Solids* **50**, 2237 (2002).
- [61] J. C. Crocker and D. G. Grier, *J. Colloid Interface Sci.* **179**, 298 (1996).
- [62] R. L. Blakeley, E. C. Webb, and B. Zerner, *Biochem.* **8**, 1984 (1969).
- [63] N. D. Jespersen, *J. Am. Chem. Soc.* **97**, 1662 (1975).
- [64] P. M. Blanco, J. L. Garcés, S. Madurga, and F. Mas, *Soft Matter* **14**, 3105 (2018).
- [65] E. Vilaseca, A. Isvoran, S. Madurga, I. Pastor, J. L. Garcés, and F. Mas, *Phys. Chem. Chem. Phys.* **13**, 7396 (2011).
- [66] K. D. Kihm, A. Banerjee, C. K. Choi, and T. Takagi, *Exp. Fluids* **37**, 811 (2004).
- [67] L. P. Fauchaux and A. J. Libchaber, *Phys. Rev. E* **49**, 5158 (1994).
- [68] S. H. Behrens and M. Borkovec, *J. Phys. Chem. B* **103**, 2918 (1999).
- [69] W. L. W. Hau, D. W. Trau, N. J. Sucher, M. Wong, and Y. Zohar, *J. Micromech. Microeng.* **13**, 272 (2003).
- [70] J. Szymański, A. Patkowski, A. Wilk, P. Garstecki, and R. Holyst, *J. Phys. Chem. B* **110**, 25593 (2006).
- [71] A. Kasper, E. Bartsch, and H. Sillescu, *Langmuir* **14**, 5004 (1998).
- [72] E. R. Weeks and D. A. Weitz, *Chem. Phys.* **284**, 361 (2002).
- [73] J. A. Dix and A. S. Verkman, *Annu. Rev. Biophys.* **37**, 247 (2008).
- [74] T. J. Feder, I. Brust-Mascher, J. P. Slattery, B. Baird, and W. W. Webb, *Biophys. J.* **70**, 2767 (1996).
- [75] K. Jacobson, A. Ishihara, and R. Inman, *Ann. Rev. Physiol.* **49**, 163 (1987).
- [76] M. R. Horton, F. Höfling, J. O. Rädler, and T. Franosch, *Soft Matter* **6**, 2648 (2010).
- [77] M. J. Saxton, *Biophys. J.* **103**, 2411 (2012).
- [78] M. J. Saxton, *Biophys. J.* **66**, 394 (1994).
- [79] M. J. Saxton, *Biophys. J.* **92**, 1178 (2007).
- [80] M. J. Saxton and K. Jacobson, *Annu. Rev. Biophys. Biomol. Struct.* **26**, 373 (1997).
- [81] T. Kosztolowicz, K. Dworecki, and S. Mrówczyński, *Phys. Rev. Lett.* **94**, 170602 (2005).
- [82] A. Srivastava and G. Krishnamoorthy, *Arch. Biochem. Biophys.* **340**, 159 (1997).